IMECE2020-23816

INVESTIGATING THE SENSITIVITY OF PARTICLE SIZE DISTRIBUTION ON PART GEOMETRY IN ADDITIVE MANUFACTURING

Vaishak Ramesh Sagar[*]
Department of Industrial and
Materials Science
Chalmers University of Technology
SE-412 96 Gothenburg
Sweden

Samuel Lorin
Johan Göhl
Johannes Quist
Christoffer Cromvik
Andreas Mark
Klas Jareteg
Fredrik Edelvik
Computational Engineering and Design
Fraunhofer Chalmers Centre
SE-412 58 Gothenburg
Sweden

Kristina Wärmefjord
Rikard Söderberg
Department of Industrial and
Materials Science
Chalmers University of Technology
SE-412 96 Gothenburg
Sweden

ABSTRACT

Selective laser melting process is a powder bed fusion additive manufacturing process that finds applications in aerospace and medical industries for its ability to produce complex geometry parts. As the raw material used is in powder form, particle size distribution (PSD) is a significant characteristic that influences the build quality in turn affecting the functionality and aesthetics aspects of the end product. This paper investigates the effect of PSD on deformation for 316L stainless steel powder, where three coupled in-house simulation tools based on Discrete Element Method (DEM), Computational Fluid Dynamics (CFD), and Structural Mechanics are employed. DEM is used for simulating the powder distribution based on the different particle size distribution of the powder. The CFD is used as a virtual test bed to determine thermal parameters such as density, heat capacity and thermal conductivity of the powder bed viewed as a continuum. The values found as a stochastic function of the powder distribution is used to test the sensitivity of the melted zone and distortion using Structural Mechanics. Results showed significant influence of particle size distribution on the packing density, surface height, surface roughness, the stress state and displacement of the melted zone. The results will serve as a catalyst in developing geometry assurance strategies to minimize the effect of particle size distribution on the geometric quality of the printed part.

Keywords: Selective laser melting, Particle size distribution, Geometric variation, 316L stainless steel, Multi-physics modelling

NOMENCLATURE

AM   Additive Manufacturing
PSD   Particle Size Distribution
DEM   Discrete Element Method
SLM   Selective Laser Melting
CFD   Computational Fluid Dynamics
PBD   Powder Bed Density
L-PBF   Laser Powder Bed Fusion
CUDA   Compute Unified Device Architecture
GPU   Graphics Processing Unit
BVH   Bounding Volume Hierarchy
FCC   Fraunhofer Chalmers Centre

---

[*]Address all correspondence to this author.

1 INTRODUCTION

Additive manufacturing (AM) is an emerging manufacturing technique that has had a large impact on the manufacturing industry thus far. This process has a number of advantages in comparison to traditional manufacturing techniques. For example, the part geometry is much freer and there is no costly tool building required. Laser powder bed fusion (L-PBF) techniques such as the SLM process enable efficient utilization of the powder as the unused powder can be recycled and reused. As the process consists of melting the raw material in powder form, the powder material characteristics are of prime importance in achieving the desired geometric quality. Particle size distribution (PSD) of the powder material is an important characteristic as it affects the final part properties.

Numerous experimental and simulation based research work on the influence of particle size distribution have been carried out. Examining variation in PSD of Ti6Al4V from three different suppliers revealed uni-modal distribution from two suppliers while the third one showed bi-modal distribution [1]. Intricate surfaces and previously solidified layer thickness were found to be the cause of variation in PSD in [2]. The effect of different particle size distribution on the PBD in [3], the influence of uni-modal and bi-modal PSD on density, microstructure and mechanical properties in 316L [4] present encouraging results.

Advancements on the simulation front have been able to mimic various aspects of the SLM process to a larger extent. Transport phenomena for multi-layer single track was simulated in [5] to predict transient variation of the melt pool and solidified build geometry during deposition. Powder variation was considered and a detailed simulation was integrated for better prediction. The work in [6] simulated the influence of PBD on the sensitivity of relative density of Ti6Al4V built parts. A comprehensive review of computational modeling in [7] concludes promising simulation prospects in capturing evolution of the phenomenon.

1.1 Scope of The Paper

In summary of the above referred works, there exists thorough experimental investigation on the influence of PSD on the build's surface quality and the mechanical properties for various metal powders. However, knowledge on how the effect of PSD translates to the build's geometric accuracy is limited. Also, there is an increased interest towards integrating various simulation tools to capture such effects. Therefore, in this paper the effect of PSD on the build geometry is examined by integrating various simulation tools that replicate the multi-physics aspects of the metal AM process.

Design of Experiments approach is employed to investigate the effect of PSD on the build geometry. Three in-house simulation tools based on Discrete Element Method (DEM), Computational Fluid Dynamics (CFD), and Structural Mechanics are employed to generate the powder distribution, heat transfer, and

displacement respectively. Packing density, surface height, surface roughness, displacement are the responses measured from simulation results. powder bed with single layer consisting of two melt tracks is simulated in this paper. However, learnings from this study will serve in setting up modelling and simulation to investigate multi layer - multi track builds. The approach of combining three simulation tools establishes a way to calculate the effect various aspects on the build geometry, that could be used in scenarios that require detailed simulation accuracy.

The paper is arranged as follows. Section 2 presents theoretical aspects of the SLM process, concept of robust design as well as background on the three in-house simulation tools. Experimental details at each step is described in Section 3. Section 4 presents the results and interpretation of the results. Section 5 concludes the paper.

2 THEORY

In this section, theoretical background on selective laser melting process and concept of robust design is given. Also, the principles of in-house built DEM, CFD and structural mechanics simulation are described.

2.1 Selective laser melting

In Selective Laser Melting (SLM) process, the powder material is applied in the form of a layer on the build platform (Fig. 1). The laser source melts the powder and fuses the powder particles together. The powder is selectively melted in the layer as per a defined laser melt path (i.e. scan pattern) and the process is repeated layer by layer by lowering the build platform. The build platform is lowered as per the required layer thickness and a roller or a recoater applies a new layer of powder material. Once the build is complete, the build is removed from the build platform for further processing based on the end requirements.
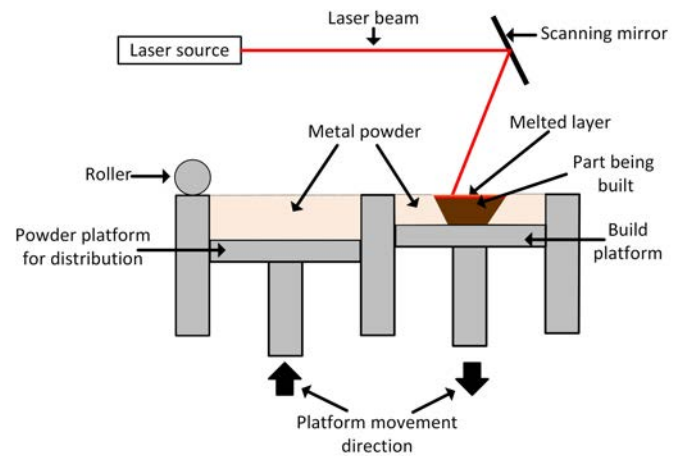

FIGURE 1: Selective Laser Melting Process

In a powder bed fusion process, PSD is a powder characteristic that influences density, mechanical properties, and surface quality. PSD requires to be engineered to the specific AM process. For example, as the powder layer shrinks after melting and solidification, the thickness of the subsequent powder layer increases. For a smaller powder layer thickness, inappropriate PSD could cause porosity and affect the overall build quality [8].

2.2 Robust Design

Geometric variation occurs in every manufacturing process and additive manufacturing process is no different. Variation in the manufacturing process parameters can cause inconsistencies between the design specifications (input) and the fabricated product (output). Reducing process variation to minimize their effect on the product's geometry is a complex and an expensive approach. Instead, a cost effective alternative would be to minimize the effect of process variation on the product's geometry. From a robust design perspective, the objective is to improve the quality of the product or the process by minimizing the effect of the causes of variation without eliminating the causes [9].

A product or a process is considered as a system as shown in the block diagram (Fig. 2). The response or the output of the system denoted as y is the performance obtained. The system's performance is influenced by a number of factors. They are classified as signal factors (M), noise factors (x), and control factors (z). Signal factors represent the desired outcome from the system. Noise factors are uncontrollable parameters which cause variation in the system's response. Noise factors affecting the system's response could be some external factors such as operating environment, wear on usage, or internal factors such as system imprecision causing variation in system's response (unit-unit). Control factors are the parameters that could be adjusted to minimize the influence of noise factors and achieve the desired outcome.

In order to minimize the effect of variation, identifying the sources of variation and understanding their influence on the build geometry is necessary. In the context of this paper, the stochastic nature of powder's PSD is treated as a variation source and its influence on the build geometry is examined.

2.3 Discrete element model

The discrete element method (DEM) is used for simulating large populations of particles such as powders, granules, rock and ore particles and many other materials. The DEM was originally proposed by Cundall and Strack in a series of publications [10] and has since been further developed by a wide range of contributors spanning many different fields of engineering and science.

DEM is a numerical method based on Newtonian interactions of a system of particles where constitutive relations including contacts and collisions, heat transfer, inter-particle bonds and forces and reaction to external fields are resolved. The DEM simulations in this paper are performed in the DEM solver
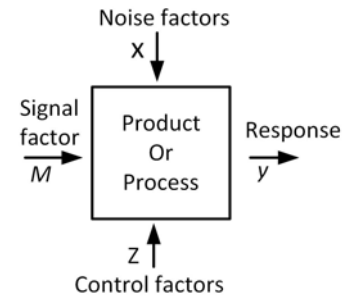
FIGURE 2: P-diagram, redrawn from [9]

Demify^{TM} developed at the Fraunhofer-Chalmers Centre (FCC). Demify^{TM} is a state-of-the-art DEM solver built to utilize the advantage of parallel processing power of GPUs using the CUDA parallel computing platform.

2.4 CFD

A computational fluid dynamics software, IPS IBOFlow® is used to simulate the melt pool dynamics of the SLM process. IPS IBOFlow developed at FCC is a finite volume based solver for incompressible multiphase flow which previously has been used to simulate e.g. the additive manufacturing in bio printing [11] and surface tension driven flows [12].

Navier Stokes equations, the transport equation for temperature together with the equation of the volume fraction advection are solved each time step. The equations are discretized on a cartesian octree grid which can be dynamically refined and coarsened to enhance or reduce the resolution of the flow if necessary. This is convenient in flows which require a refined mesh at local areas, such as the interface between metal and gas.

The laser is modeled using a ray tracing algorithm, where a circular pattern of rays based on the laser diameter are directed from a moving laser source on the powder bed. The viscosity of the fluid metal is allowed to decrease with increasing temperature, which is modeled with the Arrhenius equation. The specific heat capacity of the metal is based on the phase. Phase change is accounted for by adding the enthalpy of fusion to the specific heat capacity over the temperature interval between the solidus temperature and the liquidus temperature. To account for possible boiling, the enthalpy of vaporization is added to the specific heat capacity after the boiling point. The surface tension model used is temperature dependent and therefore has a tangential component to be able to model the Marangoni flow.

2.5 Structural Mechanics

To simulate how the solidified material distorts and to predict the resulting strain and stress fields evolve as a result of the temperature and melting and solidification, the finite element method (FEM) is used. The FEM approach for thermo-mechanical simulation of the AM process stems from welding

simulation due to many similarities between welding and metal additive manufacturing simulations [13] .

In this article, structural mechanics solver "LaStFEM" developed at FCC is used as the structural solver to perform the thermo-mechanical simulations. The material model is an elasto-plastic with temperature dependent material parameters. The constitutive model is based on infinitesimal strain theory and the melted material is modelled using the silent approach, meaning that the material points that are not solid are given a compliant material property so as to not interfere with the solid part of the geometry while ensuring that the finite element mesh is intact and not too deformed, see [13]. This is done by setting the Young's modulus to the value at the liquidation temperature for air and liquid metal.

Structural mechanics simulation captures how the powder melts, how the melt pool develops, how the pool is solidified and how the shrinkage occurs.

3 EXPERIMENTAL SETUP

In this section, details of the powder material and input parameters at each simulation stage are explained. Figure 3 illustrates the sequence of steps followed as well as the interaction of the simulation tools in this experimental setup.
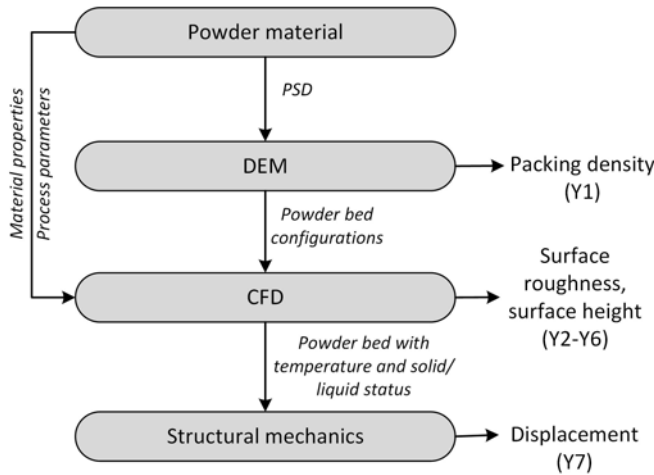

FIGURE 3: Sequence of steps in the experimental setup

The DEM simulations are first run to generate powder bed configurations for the chosen particle size distribution. The powder bed configurations along with the powder material properties and process parameters serve as input to the CFD simulations. The outcome of CFD simulations with information of powder bed with the solid/liquid status assists structural mechanics simulation to capture the process of melting, solidification, and deformation. The responses from each of these simulation stages are shown on the right side in the Figure 3.

3.1 Powder Material

316L powder is used as the reference material. It is an austenitic stainless steel offering superior corrosion resistance and is a preferred material for elevated temperature based applications. Table 1 provides the chemical composition breakdown.

TABLE 1: Chemical composition of 316L (wt.%)

Cr	Si	Mn	Ni	Mo	Fe	C	S	O	N
16.5	0.45	1.2	11	2.2	Bal	0.012	0.029	0.069	0.098

Typical particle size distribution data from a manufacturer has been used as a basis for forming a set of size distribution variants to investigate. The characteristic sizes of the reference distribution are $x_{10} = 16.3$ μm, $x_{16} = 21.0$ μm, $x_{50} = 34.5$ μm, $x_{84} = 47.9$ μm, $x_{90} = 50.9$ μm and $x_{99} = 67.4$ μm. The standard deviation of the distribution has been estimated to $\sigma_{div} = 13.5$ μm. Here, the x_{10} and x_{90} values correspond to particle size diameter that account for ten percent and ninety percent of the powder PSD respectively. For simplicity, Gaussian normal distributions are used for generating the required distribution functions for the powder bed simulations in DEM.

3.2 Design of Experiments

Design of Experiments (DOE) method was opted in this study. Four input factors were of interest namely, particle mean size in the PSD, standard deviation, laser power, and hatch spacing. Laser scan speed and beam diameter were kept constant at 1000 mm/s and 0.05 mm respectively. The powder layer thickness was chosen to be 67.4 $\mu m(x_{99})$. Table 2 provides details of the factors and their levels.

TABLE 2: Factors and their levels in DOE configuration

Label	Factor	-1	0	+1
X1	Mean size, $x_{50}(\mu m)$	21.1	34.6	48.0
X2	Standard Deviation, $\sigma_{dev}(\mu m)$	2.7	13.5	24.2
X3	Laser power, P (W)	100	150	200
X4	Hatch spacing, $H_s(\mu m)$	50	70	90

A full factorial design was considered with four factors, each at two levels as specified above. In addition, three runs at reference value were made for purpose of comparison. Table 3 and Fig. 4 provide details of the DOE configuration.

3.3 DEM case configuration

Powder particles were generated in a domain above the intended bed and were allowed to free fall and settle, see Fig. 5. It must be noted that this configuration does not consider a recoater
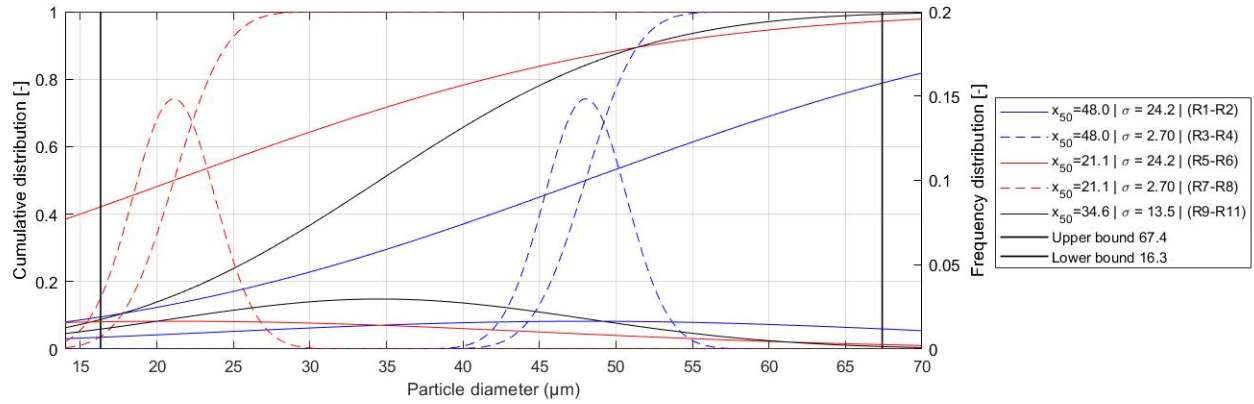
FIGURE 4: Powder particle size distributions as simulated in the DOE configuration

TABLE 3: DOE matrix

Runs	X1	X2	X3	X4	Runs	X1	X2	X3	X4
1	-1	-1	-1	-1	11	1	-1	1	-1
2	-1	-1	-1	1	12	1	-1	1	1
3	-1	-1	1	-1	13	1	1	-1	-1
4	-1	-1	1	1	14	1	1	-1	1
5	-1	1	-1	-1	15	1	1	1	-1
6	-1	1	-1	1	16	1	1	1	1
7	-1	1	1	-1	17	0	0	0	0
8	-1	1	1	1	18	0	0	0	0
9	1	-1	-1	-1	19	0	0	0	0
10	1	-1	-1	1					

TABLE 4: Parameters used in DEM simulation

Parameter	Value	Unit
Solid density, ρ_s	7269	kg/m^3
Static friction p-p, μ_s	0.4	-
Static friction p-w, μ_s	0.4	-
Rolling friction p-p, μ_r	0.005	-
Rolling friction p-w, μ_r	0.005	-
Surface energy p-p, γ	0.1	mJ/m^2
Young's Modulus, E	200e6	Pa
Poisson's ratio, ν	0.294	-
Time-step, dt	8.7e-8	s

or a roller to spread the powder on the build platform. However, the free fall approach replicates stochastic nature of the powder distribution. Material model parameters and simulation settings are provided in Table 4. The powder PSD is set according to a truncated normal distribution with mean and standard deviation values according to the DOE setup in Table 3. An illustration of different powder packing configurations is provided in Fig. 6.

3.4 CFD

The parameter values for 316L used in CFD simulation were obtained from [14, 15] and are tabulated in Table 5. Same material was chosen for the substrate as well. The size of computational domain was set to 1mm × 0.3mm × 0.4mm. The computational grid was dynamically refined to enhance the resolution of the metal surface, where the finest grid size used was 6.25μm. A constant time step of 0.1μm was used in the simulations. Two tracks were melted with each track length measuring 0.8 mm. Figure 7 illustrates the CFD simulation of the melt pool.
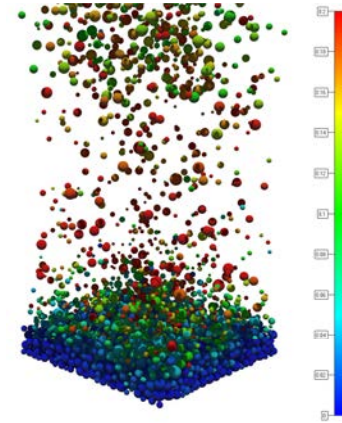

FIGURE 5: Snapshot of the filling procedure of the particle bed formation. Particles colored by velocity (color-map unit in m/s)

3.5 Structural Mechanics

The temperature and solid/liquid status of the material at different points are extracted from CFD simulation to calculate the stress and strain fields and the resulting displacement. The bot-
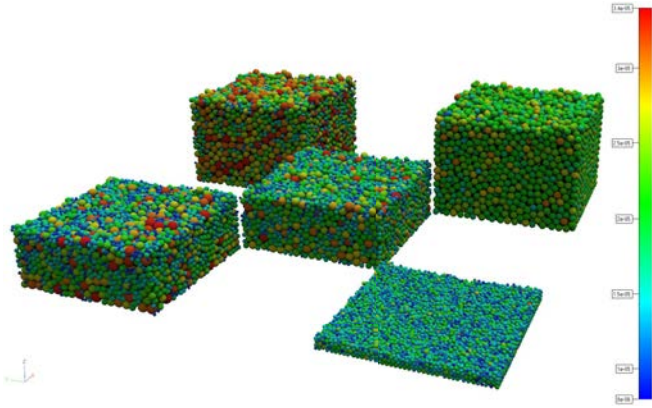
FIGURE 6: Illustration of the five different powder particle packing configurations simulated. Particles colored by radius.

TABLE 5: Parameters used in the CFD simulation

Parameter	Value	Unit
Density, ρ_s	7269	kg/m^3
Density, ρ_l	6881	kg/m^3
Viscosity, η	0.008	Pa.s
Specific heat capacity, $C_{p(s)}$	688.6	J/(kg.K)
Specific heat capacity, $C_{p(l)}$	773.7	J/(kg.K)
Thermal conductivity, $k_{(s)}$	32.17	W/(m.K)
Thermal conductivity, $k_{(l)}$	27.5	W/(m.K)
Liquidus temperature, T_l	1723	K
Solidus temperature, T_s	1658	K
Enthalpy of fusion, ΔH_f	260	kJ/kg
Boiling point, T_b	3090	K
Enthalpy of vaporization, ΔH_v	7406	kJ/kg
Emissivity, ε	0.36	K
Surface tension, γ	1.76	N/m

tom of the base plate is locked from translation in z-direction, the point $(0,0,0)$ is locked from translation in *x*- and *y*-direction and finally the point $(1,0,0)$ is locked from translation in the *x*-direction.

In Fig. 8, the geometry is depicted when laser has melted the track on the right side. Here, only the part of the computational model that is solid is shown. In a cross section it is seen how the equivalent plastic strain (top right) and the von Mises stress (bottom right) is growing as the structure is cooling down. These fields depend on how the geometry was melted.

4 RESULTS AND DISCUSSION

In this section, outcome from each simulation step is presented and discussed. To accurately resolve the melting-, melt pool-, and solidification dynamics in CFD simulations, the time step needs to be correctly adjusted. During the course of this pa-
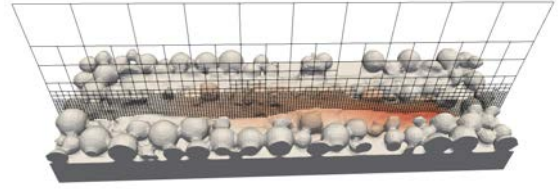

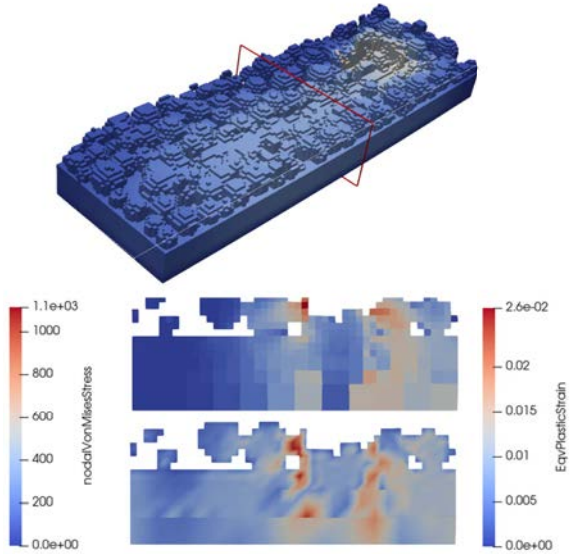FIGURE 7: A CFD simulation of the melt pool with a slice of the computational grid used is shown.

FIGURE 8: A thermo-mechanical simulation that is coupled to the CFD simulation. To the right above is a cross section of equivalent plastic strain and below von Mises stress.

per, it was learnt through iterations that the number of time steps to capture the complete melting and solidification was higher than initially anticipated. As a consequence, this lead to incomplete structural simulation runs - R3, R4, R7, R8, R11, R12, R15, R16, R17, R18, and R19. Hence, the discussion will revolve around the completed runs. Table 6 summarizes the results.

4.1 Results from Powder, melt pool dynamics, and structural mechanics simulations

The powder bed simulation was successful for all the runs from DEM simulations. Here, packing density (Y1) was observed as the response. CFD simulations served as the source for capturing the mean layer height and surface roughness information. Mean layer height (Y2), standard deviation (Y3), surface roughness components such as the arithmetic average roughness R_a (Y4), the maximum valley depth below the surface mean line

TABLE 6: Design of experiments table and response measurement values

Runs	X1	X2	X3	X4	Y1 (RoH0)	Y2 (Zmean)	Y3 (Zstd)	Y4 (Ra)	Y5 (Rv)	Y6 (Rp)	Y7 (Zdisp)
R1	-1	-1	-1	-1	0.5522	49.5295	2.2618	1.5796	31.12	59.75	5.6169
R2	-1	-1	-1	1	0.5522	50.1659	3.1864	2.1946	32.01	64.53	6.1665
R3	-1	-1	1	-1	0.5521	45.8752	3.2146	2.8463	34.75	55.78	-
R4	-1	-1	1	1	0.5521	45.4216	3.4655	2.961	34.75	61.22	-
R5	-1	1	-1	-1	0.565064	36.3193	2.9948	2.0874	16	53.5	6.5019
R6	-1	1	-1	1	0.565064	37.4441	7.5456	5.6632	16	62.02	6.0072
R7	-1	1	1	-1	0.568458	30.1907	2.2897	1.3802	23.82	57.11	-
R8	-1	1	1	1	0.568458	31.1119	1.4077	0.73126	22.25	42.6	-
R9	1	-1	-1	-1	0.57353	30.6647	2.6646	1.7386	7.14	47.25	6.1927
R10	1	-1	-1	1	0.57353	32.2946	4.9922	3.4478	16	59.51	6.2672
R11	1	-1	1	-1	0.575219	26.1131	1.8922	1.429	22.25	41	-
R12	1	-1	1	1	0.575219	26.8609	1.4584	0.82712	19.9	39.33	-
R13	1	1	-1	-1	0.58389	33.5232	3.5512	2.4922	22.25	59.75	5.9764
R14	1	1	-1	1	0.58389	34.8144	5.8835	4.3938	17.63	54.3	5.88
R15	1	1	1	-1	0.586277	30.5623	1.7474	1.214	25.18	49.67	-
R16	1	1	1	1	0.586277	31.0212	3.46494	1.462	25.05	57.86	-
R17	0	0	0	0	0.570994	30.7731	1.9356	1.3692	22.25	47.25	-
R18	0	0	0	0	0.576778	31.0986	1.9804	1.3495	19.3	47.25	-
R19	0	0	0	0	0.562401	31.0867	1.8854	1.2988	22.25	41	-

TABLE 7: Sensitivity analysis results showing individual p-values for each main source and their interaction

	Effect- PValue					
Source	Y1	Y2	Y3	Y4	Y5	Y6
X1	0.0001	0.0001	0.8939	0.54705	0.0083	0.15191
X2	0.0001	0.0007	0.30845	0.55323	0.07231	0.77764
X3	0.02	0.00012	0.03856	0.03607	0.01258	0.1047
X4	1	0.1288	0.08676	0.12681	0.93746	0.56233
X1.X2	0.0015	0.0001	0.77506	0.64706	0.00176	0.08553
X1.X3	0.5591	0.2918	0.5901	0.39254	0.52596	0.74186
X1.X4	1	0.61044	0.83699	0.91988	0.85949	0.76092
X2.X3	0.0203	0.8216	0.17599	0.06402	0.94439	0.70436
X2.X4	1	0.7383	0.40141	0.43042	0.34268	0.43428
X3.X4	1	0.429	0.1205	0.06979	0.5145	0.45987

R_v (Y5), the maximum peak height above the surface mean line R_p (Y6) were extracted as responses from CFD simulations.

Figure 9 presents a sample result of the surface map (from R1) and plots showing Y2 and Y3 responses. Figure 10 presents a sample visualization of layer height, surface temperature, and melt pool in CFD simulation for the completed runs. From the structural simulations, displacement along the Z direction of the tracks (Y7) was captured for the completed runs. Also, the stress state in the contact area of the melted tracks and build platform was observed and is presented in Figure 11.

4.2 Discussion

The results from the analysis is tabulated in Table 7. The Y1 packing density response is complete since it is solely calculated from the DEM powder bed simulation. The results suggest a significant effect of mean particle size (X1) as well as the standard deviation (X2) on packing density. As shown in table 6, even though the difference in packing density is relative small among all the runs, it can be observed that a wider particle size distribution leads to higher packing density. The analysis also indicates that the input factors X1, X2, along with laser power settings (X3) have an effect on the Y2 response (mean layer height). These observations made on the effect of PSD are in agreement with experimental studies conducted in studies within this research framework.

The effect of hatch spacing and the PSD on the resulting stress state in the contact region of the melted zone and the build platform can be seen in Figure 11. For example in R1, owning to the narrow PSD and low hatch spacing settings, the two melt
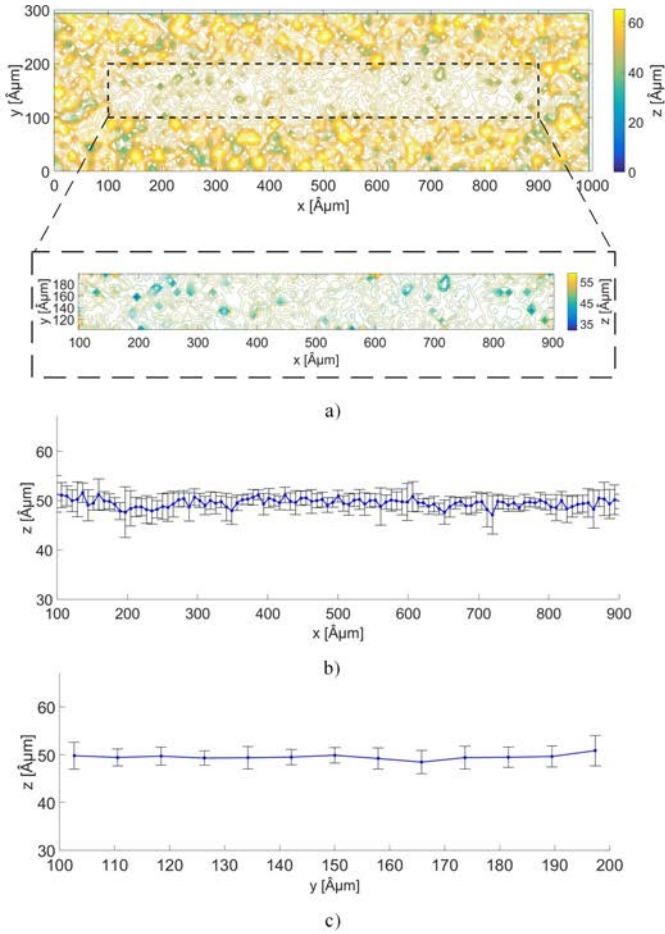
FIGURE 9: From R1, a) Surface contour plot with magnified region highlighting the melted area. b) Mean layer height plot along the melt track and, c) mean layer height across the melt track.

tracks fuse together with the fusion of powder particles more evident on the right side of the powder bed (as shown). This occurs because the laser heat source transits from the first track to the second track. Therefore, the stress is built up along the boundaries of the melted area. The distinctive gap of the track boundaries on the left side of the powder bed (as shown) could mean unmelted zone, which is more clearly visible in R2. Due to the higher hatch spacing in R2, results in gap between the melted tracks and leads to unmelted powder particles and porosity.

Contrary to runs R1 and R2, the runs R13 and R14 have wider PSD. The effect of wider PSD is evident in the color mapping of the stress state along the boundaries of the melted zone and the track boundaries. Bigger mean particle size with lower power settings and higher hatch spacing settings causes partial melting of the powder particles between the melting tracks as clearly shown in in Fig. 10.
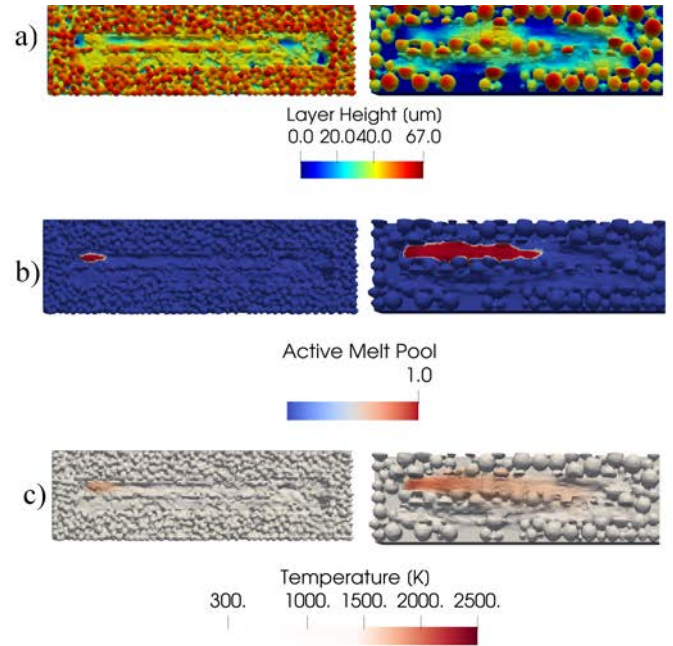

FIGURE 10: Visualization of runs R1 and R16 as an example showing a) Layer height, b) Surface temperature, and c) Active melt pool from end of CFD simulations.

5 CONCLUSION AND FUTURE WORK

Additive manufacturing of metals is being vastly adapted within various industries. Utilizing its potential to the fullest requires understanding of various factors in the process that contribute to the build quality. Influence of metal powder characteristics such as the particle size distribution is one such factor that requires to be well understood. With this being the objective, effect of particle size distribution on the build geometry was examined in this paper. This was performed by integrating the in-house built DEM, CFD and structural mechanics simulation platforms. The effect of particle size distribution on packing density, mean layer height were observed to be significant. Also, it was observed that the particle size distribution influenced the resulting stress buildup at the melted area. In addition to the above findings, the prospect of integrating simulation tools to investigate various aspects of metal additive manufacturing was found to be promising.

The outcome of this work will pave way for many future activities. Performing a multi-layer, multi-track melting simulation will enable to capture the effect of PSD and layer thickness at a larger scale. Also, the scope will be further expanded as per the robust design methodology where various factors will be classified into control factors and noise factors. Optimizing the control factors such as the build direction, scanning strategy, layer thickness, support structures by considering effect of noise factors such as chemical composition, particle size distribution etc. will be studied. A long term objective is to consider these build
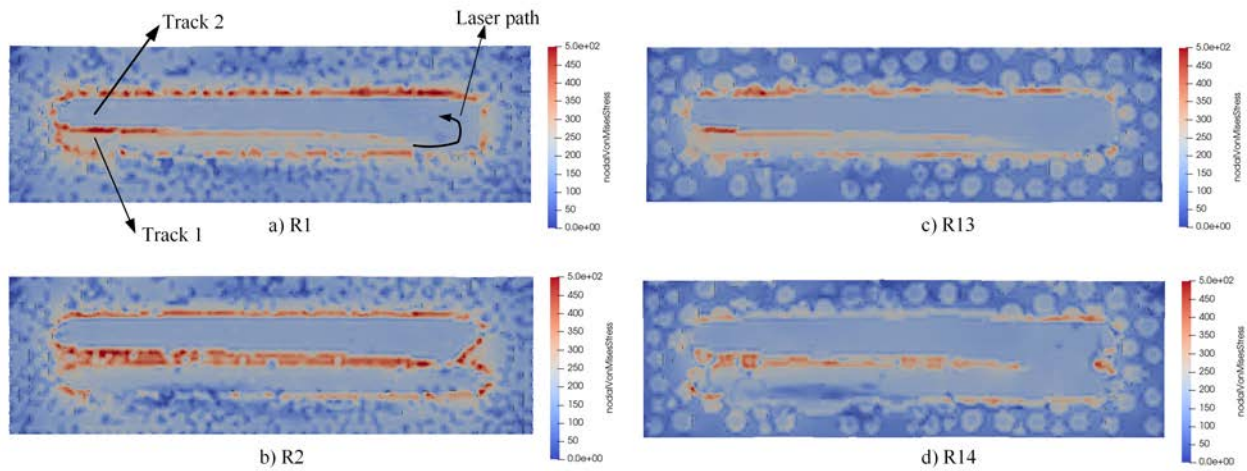
FIGURE 11: Visualization of final stress state in the runs R1, R2, R13 and R14 as an example from structural simulations.

level effects while planning part positioning and fixture design aspects in hybrid manufacturing scenarios. However in order to perform the above mentioned activities, long simulation times and high cost incured will have to be handled. Hence, faster simulation techniques will also be explored.

REFERENCES

[1] Gu, H., Gong, H., Dilip, J., Pal, D., Hicks, A., Doak, H., and Stucker, B., 2014. "Effects of powder variation on the microstructure and tensile strength of ti6al4v parts fabricated by selective laser melting". In Proceedings of the 25th annual international solid freeform fabrication symposium, austin, tx, usa, pp. 4–6.

[2] Whiting, J., and Fox, J., 2016. "Characterization of feedstock in the powder bed fusion process: sources of variation in particle size distribution and the factors that influence them". In International Solid Freeform Fabrication Symposium, Austin, Texas, USA.

[3] Jacob, G., Jacob, G., Brown, C. U., and Donmez, A., 2018. *The influence of spreading metal powders with different particle size distributions on the powder bed density in laser-based powder bed fusion processes*. US Department of Commerce, National Institute of Standards and Technology.

[4] Coe, H. G., and Pasebani, S., 2020. "Use of bimodal particle size distribution in selective laser melting of 316l stainless steel". *Journal of Manufacturing and Materials Processing,* **4**(1), p. 8.

[5] Lee, Y., and Zhang, W., 2016. "Modeling of heat transfer, fluid flow and solidification microstructure of nickel-base superalloy fabricated by laser powder bed fusion". *Additive Manufacturing,* **12**, pp. 178–188.

[6] Rausch, A. M., Küng, V. E., Pobel, C., Markl, M., and Körner, C., 2017. "Predictive simulation of process windows for powder bed fusion additive manufacturing: Influence of the powder bulk density". *Materials,* **10**(10), p. 1117.

[7] Liu, J., Jalalahmadi, B., Guo, Y., Sealy, M. P., and Bolander, N., 2018. "A review of computational modeling in powder-based additive manufacturing for metallic part qualification". *Rapid Prototyping Journal*.

[8] Dawes, J., Bowerman, R., and Trepleton, R., 2015. "Introduction to the additive manufacturing powder metallurgy supply chain". *Johnson Matthey Technology Review,* **59**(3), pp. 243–256.

[9] Phadke, M. S., 1995. *Quality engineering using robust design*. Prentice Hall PTR.

[10] Cundall, P. A., and Strack, O. D. L., 1979. "A discrete numerical model for granular assemblies". *Géotechnique,* **29**(1), pp. 47–65.

[11] Göhl, J., Markstedt, K., Mark, A., Håkansson, K., Gatenholm, P., and Edelvik, F., 2018. "Simulations of 3d bio-

printing: predicting bioprintability of nanofibrillar inks".
Biofabrication, **10**(3), p. 034105.

[12] Göhl, J., Mark, A., Sasic, S., and Edelvik, F., 2018. "An immersed boundary based dynamic contact angle framework for handling complex surfaces of mixed wettabilities". *International Journal of Multiphase Flow,* **109**, pp. 164–177.

[13] Gouge, M., and Michaleris, P., 2017. *Thermo-mechanical modeling of additive manufacturing.* Butterworth-Heinemann.

[14] Kim, C. S., 1975. Thermophysical properties of stainless steels. Tech. rep., Argonne National Lab., Ill.(USA).

[15] Mills, K. C., 2002. *Recommended values of thermophysical properties for selected commercial alloys.* Woodhead Publishing.